

NeuralDiffuser: Controllable fMRI Reconstruction with Primary Visual Feature Guided Diffusion

Haoyu Li¹ Hao Wu² Badong Chen¹

Abstract

Reconstructing visual stimuli from functional Magnetic Resonance Imaging (fMRI) based on Latent Diffusion Models (LDM) provides a fine-grained retrieval of the brain. A challenge persists in reconstructing a cohesive alignment of details (such as structure, background, texture, color, etc.). Moreover, LDMs would generate different image results even under the same conditions. For these, we first uncover the neuroscientific perspective of LDM-based methods that is top-down creation based on pre-trained knowledge from massive images but lack of detail-driven bottom-up perception resulting in unfaithful details. We propose NeuralDiffuser which introduces primary visual feature guidance to provide detail cues in the form of gradients, extending the bottom-up process for LDM-based methods to achieve faithful semantics and details. We also developed a novel guidance strategy to ensure the consistency of repeated reconstructions rather than a variety of results. We obtain the state-of-the-art performance of NeuralDiffuser on the Natural Senses Dataset (NSD), which offers more faithful details and consistent results.

1. Introduction

Decoding visual stimuli from brain activation, such as the functional Magnetic Resonance Imaging (fMRI), is a promising technology in the field of neuroscience. It not only uncovers the intricate visual cognitive processes of the brain (Güçlü & van Gerven, 2015; Wen et al., 2018; Kietzmann et al., 2019), but also holds the potential to significantly advance the community of brain-computer interfaces (Horikawa & Kamitani, 2017; Qian et al., 2020).

¹Institute of Artificial Intelligence and Robotics, Xi'an Jiaotong University, Xi'an, China ²School of Electrical Engineering, Xi'an University of Technology, Xi'an, China. Correspondence to: Hao Wu <wuhaoacm@163.com>, Badong Chen <chenbd@mail.xjtu.edu.cn>.

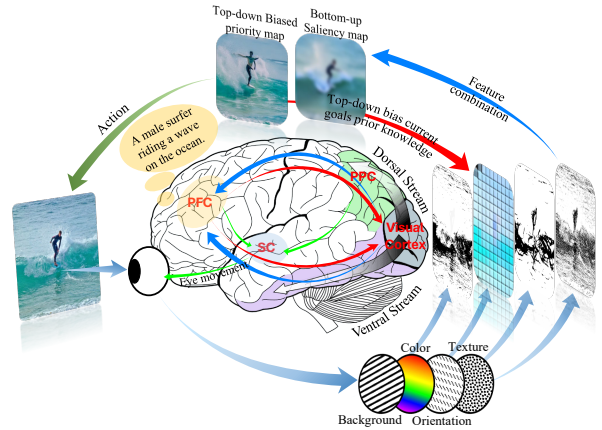


Figure 1. Schematic diagram of bottom-up and top-down processes in neuroscience. The perception of the visual scene is shaped by the reciprocal interaction of bottom-up perception, driven by visual cues from the retina (blue flows), and top-down creation, which incorporates prior knowledge and experience (red flows).

Recently, researchers have shown a keen interest in a captivating decoding task that aims to reconstruct the visual stimuli perceived by subjects providing a fine-grained retrieval of the intricate connections between biological brain activity and cognitive computation. However, the task remains challenging due to the modality gap between fMRI and images. As a result, numerous pixel-to-pixel techniques result in ambiguous images and lack semantic coherence (St-Yves & Naselaris, 2018; Seeliger et al., 2018; Shen et al., 2019; Lin et al., 2019; Ren et al., 2021).

Nowadays, generative artificial intelligence, especially the Latent Diffusion Model (LDM) (Rombach et al., 2022), provide a fertile landscape for achieving remarkable advancements in fMRI reconstruction. The LDM, pre-trained on massive images learns the prior knowledge and experience, thereby generating high-quality natural images. LDMs generate images using two input embeddings: the initial latent from VQ-VAE and the condition from the CLIP shared space. In this paradigm, LDM-based methods aim to map the fMRI data to the two aforementioned embeddings.

Several studies utilized ridge regression models as fMRI decoders (Takagi & Nishimoto, 2023a; Chen et al., 2023; Ozcelik & VanRullen, 2023; Lu et al., 2023). Recent studies have demonstrated that utilizing large neural networks to map

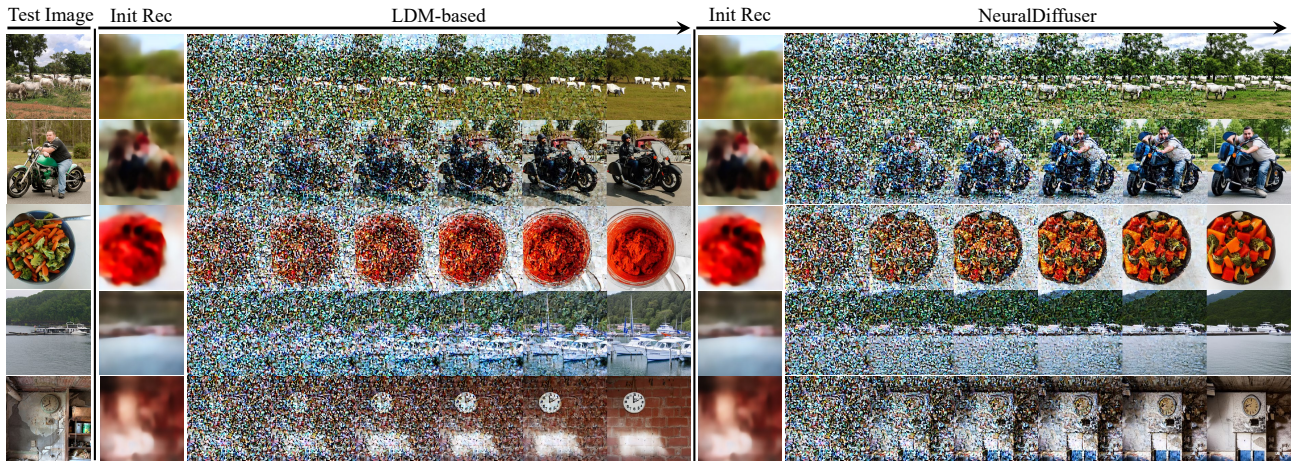


Figure 2. Reverse diffusion process of LDM-based methods (left) and NeuralDiffuser (right). Results of LDM-based methods are initialized by a blurry reconstruction and tend to produce unfaithful details. In contrast, NeuralDiffuser adopts guidance to correct the initial latent within few steps and obtain more faithful details and consistent results.

fMRI data to the two embeddings of LDMs has achieved excellent results(Scotti et al., 2023; Xia et al., 2023), providing a strong motivation for further advancements.

Despite promising results have been achieved, reconstructing faithful detail remains a challenge. To do this, MindDiffuser(Lu et al., 2023) and MindEye-BOI(Kneeland et al., 2023) repeatedly iterate reverse diffusion process to optimize two embeddings which is extremely time consuming. In addition, Takagi(Takagi & Nishimoto, 2023b) and DREAM(Xia et al., 2023) suggest that the incorporation of depth and color is beneficial to improve structural fidelity. However, these are difficult to be decoded from fMRI.

Our perspective on LDM-based fMRI reconstruction is grounded in the neuroscientific theory. As shown in Figure 1, visual cognition involves both bottom-up process, which entails passive perception of visual cues from the thalamus, and top-down process, which involves active creation by the conscious mind. The LDM-based method, reflecting the top-down process, leverages pre-trained knowledge and experience from massive images to generate images conditional on fMRI semantics, while lacking the detail-driven bottom-up process. Consequently, uncontrolled LDM results in the unfaithful details being initialized by a blurry reconstruction, which notoriously suffers from inaccurate fMRI decoding as shown in Figure 2(left). To matters worse, as generative models, LDMs inherently exhibit diversity, which leads to a variety of image results even under the same conditions(Section 4.5).

In this paper, we propose NeuralDiffuser to achieve not only meaningful semantics but also faithful details and consistent results. Specifically, NeuralDiffuser utilizes neural networks to enhance the fMRI decoder performance, particularly for high-level semantic features. In addition, drawing insight from the bottom-up process, we propose a primary visual

feature-guidance which provide detail cues for LDM in the form of gradients to control the reverse diffusion process as present in Figure 2(right). Furthermore, we have developed a novel guidance strategy to ensure the consistency of repeated generations instead of a variety of results (Section 4.5). From a neuroscience perspective, NeuralDiffuser propose primary visual features guidance, which opens up feedforward bottom-up process for providing detail cues and combine it with knowledge-driven top-down process. For a computational view, NeuralDiffuser incorporates primary visual features that are well decoded to compensate for suboptimal decoding performance on blurry initial latent (section 4.2).

Our NeuralDiffuser offers three distinct advantages. First, we propose primary visual feature guidance to control reverse diffusion process and achieved state-of-the-art in meaningful semantics, faithful detail, and consistent results. Second, we develop a novel guidance strategy to obtain consistent images, which can be extended to other reconstructions tasks. Third, the proposed method is independent of LDMs and fMRI embeddings, allowing its adopting in any existing LDM-based reconstruction approach.

Our contributions can be summarized in three aspects:

- We first provide a constructive insight into LDMs from neuroscience theory (top-down and bottom-up process) and draw the reasons for unfaithful detail of LDM-based fMRI reconstruction methods.
- We propose NeuralDiffuser which introduces primary visual feature guidance to provide detail cues for LDM-based fMRI reconstruction to achieve faithful semantics and details. We also developed a novel guidance strategy to ensure the consistency of repeated reconstructions rather than a variety of results.

- We evaluate the state-of-the-art performance of NeuralDiffuser on the Natural Scenes Dataset, comparing with previous works both quantitatively and qualitatively. We also present ablation studies and further discussion of the proposed method.

2. Related Work

2.1. fMRI Visual Stimuli Reconstruction

End-to-End: Numerous previous studies employ generative adversarial network (GAN)(Goodfellow et al., 2014), variational autoencoder(VAE)(Kingma & Welling, 2013) and self-supervised learning(Beliy et al., 2019) to achieve pixel-level reconstruction of visual stimuli(St-Yves & Naselaris, 2018; Seeliger et al., 2018; Shen et al., 2019; Lin et al., 2019; Ren et al., 2021). However, these methods face limitations due to the noise in fMRI data and fewer voxels of visual cortex than image pixels. Consequently, these methods usually result in ambiguous and non-semantic images.

Pretrained Generative Models: Deep generative models, including IC-GAN(Perarnau et al., 2016), StyleGAN(Karras et al., 2020a;b) and LDMs(Rombach et al., 2022) have been widely used in reconstruction tasks. Methods for fine-tuning pre-trained generative models to match the representations of fMRI such as Mind Reader(Lin et al., 2022). Alternatively, some methods train decoders to map fMRI to IC-GAN(Ozcelik et al., 2022) or LDMs(Takagi & Nishimoto, 2023a; Chen et al., 2023; Lu et al., 2023; Ozcelik & VanRullen, 2023). Furthermore, recent studies have demonstrated the mapping of fMRI data to LDM using a large neural network, which has yielded notable results(Scotti et al., 2023; Xia et al., 2023). NeuralDiffuser is built upon the LDM as in the above studies. Additionally, NeuralDiffuser improves the detail fidelity using primary visual feature guidance inspired by the bottom-up cognitive process.

2.2. Diffusion Models

Conditional Image Generation: Conditions(Categories or prompts) are provided to diffusion models with a classifier(Dhariwal & Nichol, 2021) or classifier-free(Ho & Salimans, 2022). Classifier guidance back-propagates gradients through additional trained classifiers that can be fed noisy images. In classifier-free guidance, the LDM is re-trained to input semantic prompts directly, thus free from multiple additional classifiers.

Guided Image Generation: To control the generated images by visual properties (such as sketch, depth map, edge map, style, color, etc.), studies train the control model to guide diffusion models(Zhang et al., 2023; Mou et al., 2023; Zhao et al., 2023). Additionally, some studies have fine-tune the UNet to input guidance using concatenation(Ju et al., 2023; Voynov et al., 2023) or cross-attention(Zheng

et al., 2023). These, however, require training of the control model or fine-tuning the diffusion models. Moreover, the guidance of visual properties are difficult to decode directly from fMRI(Takagi & Nishimoto, 2023b; Xia et al., 2023). A general guided method is proposed to extend the control function(Bansal et al., 2023). However, in our task, the guidance must be decoded from fMRI, which inevitably introduces inaccurate control and additional noise. In addition, it is crucial for repeated results to be consistent with the test images rather than varying across different images.

3. Methods

Below, we elaborate on the details of the methods involved in our proposed NeuralDiffuser. We unravel the process of human visual cognition to reveal the neuroscientific principles of LDM-based methods (Section 3.1). Visual cues are mapped from fMRI into two embeddings a.k.a the semantic condition and the initial latent of the LDM (Section 3.2). Primary visual feature guidance is proposed to obtain faithful details and consistent results (Section 3.3).

3.1. Preliminary

LDM’s Neurological Perspective: Neuroscience has unveiled the crucial role of sensation and perception in the visual cognition system(Pollen, 1999; Gilbert & Sigman, 2007). This process can be described as a combination of top-down and bottom-up process. Top-down process relies on our knowledge, experience, and expectations, while bottom-up process relies on the detailed sensory inputs, as illustrated in Figure 1. See Appendix A.1 for details.

The LDM generates images by sampling from the probability distribution $p(\mathbf{x})$. We argue that the neurological perspective of $p(\mathbf{x})$ represents the pre-trained knowledge, experience, and expectations from massive images, which motivate high quality image results in fMRI reconstruction tasks. Conditional LDM $p(\mathbf{x}|c)$ drives improvements in semantic fidelity because c is organized by high-level semantics. However, when it comes to capturing details, primary visual features such as structure, background, color, and texture are still not well reproduced because detail-driven bottom-up is not implicit in LDM. Therefore, we claim that the essence of LDM is fidelity to semantics but variety to details, while the latter may contradicts faithful details and consistent results in reconstruction tasks.

Overview: Figure 3 presents the architecture of NeuralDiffuser. FMRI reconstruction seeks to map fMRI to images $x_i \rightarrow y_i$. Since LDMs explore well-mapping from text/image embeddings to images, fMRI reconstruction task is simplified as mappings $f_z : x_i \rightarrow z_i$ and $f_c : x_i \rightarrow c_i$, where z_i denotes the initial latent representing a blurry initial reconstruction and c_i represents the semantic condition.

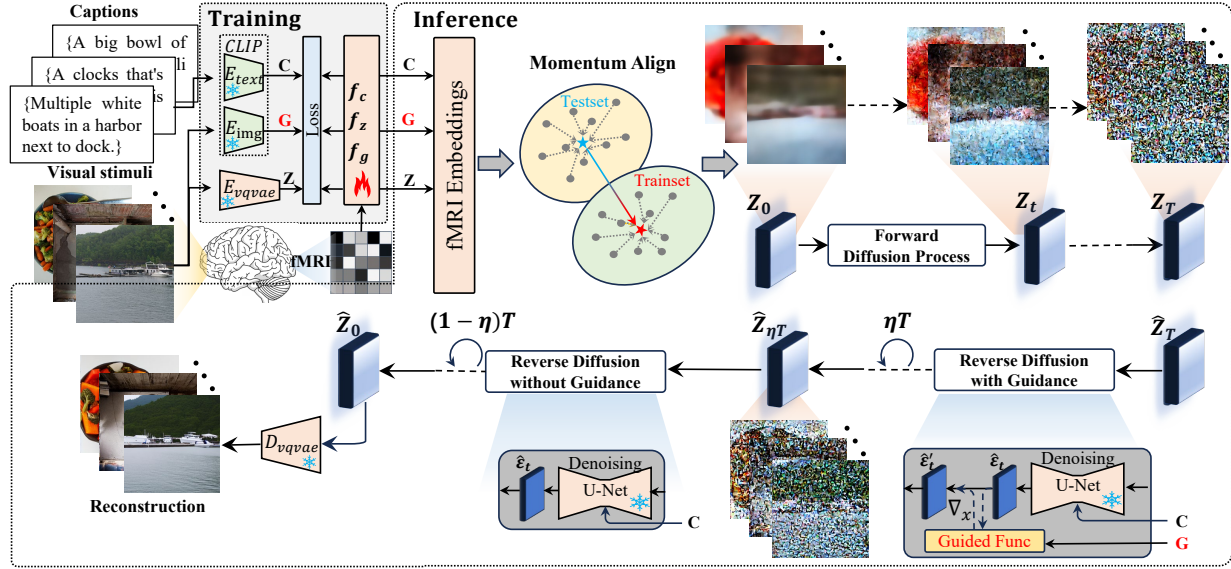


Figure 3. Architecture of NeuralDiffuser. During the training stage, the fMRI is mapped to c (CLIP text space), z (VQ-VAE’s latent space) and g (multiple layers of CLIP visual encoder). During testing, fMRI embeddings from testset is aligned to the center of the training set. Subsequently, an LDM executes a forward and reverse diffusion process with or without guidance to generate reconstructed images.

The LDM generates images conditional on z and c . Specifically, z is firstly diffused forward to a Gaussian noise z_T . A pre-trained UNet is then adopted to estimate the noise at the t -th step conditional on c and remove noise from z_t . Finally, image results are decoded from z_0 using VQ-VAE. We introduce the details of mapping x to z and c in Section 3.2. To enhance detail fidelity, we propose the primary visual feature guidance where reverse diffusion process is guided by a new mapping $f_g : x_i \rightarrow g_i$, where g is elaborately designed to represent the primary visual feature (i.e. multiple layers of the clip visual encoder). We describe the primary visual feature guided diffusion reconstruction in Section 3.3.

3.2. fMRI Embeddings Decoding

We train f_c and f_z on the data set $\{(x_i, y_i, l_i)\}_{i=1}^n$, where x_i represents fMRI recordings, y_i denotes visual stimulus and l_i is the image’s caption. The momentum alignment is adopted in the test set to keep the distribution close to the training set.

Semantic Conditional Decoding: The semantic conditions $c_i = CLIP_{text}(l_i)$ are extracted from the text space of CLIP ViT/L-14. The f_c follows the point of MindEye, which is a residual Multi-Layer Perceptron (MLP) backbone followed by a projector, and a diffusion prior to bridge the modality gap between fMRI and CLIP text space (see Appendix A.5 for details). We train MLP backbone with CLIP loss and MixCo (Kim et al., 2020) as Equation (1).

Here τ is a temperature hyperparameter, p is the pro-

jector output following MLP and $'*$ ' represents L2-normalization. Note that $P_i = \sum_{m=0}^{N-1} \exp(\frac{p_i^* \cdot c_m^*}{\tau})$ and $C_j = \sum_{m=0}^{N-1} \exp(\frac{p_m^* \cdot c_j^*}{\tau})$.

After one third of the training stage, we replace the CLIP loss with a soft CLIP loss where soft probability distributions have better supervision than hard labels.

$$\mathcal{L}_{soft} = -\frac{1}{N} \sum_{i,j=0}^{N-1} \left[\frac{\exp(\frac{c_i^* \cdot c_j^*}{\tau})}{\sum_{m=0}^{N-1} \exp(\frac{c_i^* \cdot c_m^*}{\tau})} \cdot \log \frac{\exp(\frac{p_i^* \cdot c_j^*}{\tau})}{\sum_{m=0}^{N-1} \exp(\frac{p_i^* \cdot c_m^*}{\tau})} \right] \quad (2)$$

In addition, the diffusion prior (Ramesh et al., 2022) is implemented to bridge the modality gap between fMRI and CLIP text space. The total training loss is defined as:

$$\mathcal{L}_c = \mathcal{L}_{mix|soft} + \alpha \cdot \mathcal{L}_{prior} \quad (3)$$

Initial Latents Decoding: The f_z uses a MLP backbone to map voxels to $\mathbb{R}^{64 \times 16 \times 16}$ which are upsampled to the VQ-VAE latent space $\mathbb{R}^{4 \times 64 \times 64}$. Same as f_c , the MLP backbone of f_z followed by a projector that maps the output to $\mathbb{R}^{512 \times 16 \times 16}$. The loss function of f_z consists of soft CLIP loss and Mean Absolute Error(MAE) reconstruction loss:

$$\mathcal{L}_z = \mathcal{L}_{mae} + \beta \cdot \mathcal{L}_{soft} \quad (4)$$

$$\mathcal{L}_{mae} = \frac{1}{N} \sum_{i=0}^{N-1} |\hat{z}_i - z_i| \quad (5)$$

where \hat{z} is the estimated initial latent.

$$\mathcal{L}_{mix} = -\frac{1}{N} \left[\sum_{i=0}^{N-1} \left(\lambda_i \log \frac{\exp(\frac{p_i^* \cdot c_i^*}{\tau})}{P_i} + (1 - \lambda_i) \log \frac{\exp(\frac{p_i^* \cdot c_i^*}{\tau})}{P_i} \right) + \left(\lambda_j \log \frac{\exp(\frac{p_j^* \cdot c_j^*}{\tau})}{C_j} + (1 - \lambda_j) \log \frac{\exp(\frac{p_j^* \cdot c_j^*}{\tau})}{C_j} \right) \right] \quad (1)$$

Momentum Alignment: A first-order momentum alignment is proposed to align the statistics (mean and std) of fMRI embeddings between the training and test set. We emphasize that this contributes to align the distribution center of the source and target domain. First, we normalize fMRI embeddings \hat{z} and \hat{c} on test set:

$$x' = \frac{x - \mu_x}{\sigma_x} \quad (6)$$

Next, \hat{z}' and \hat{c}' are aligned to the mean and standard deviation of the training set:

$$x'' = \sigma_{tr} \cdot x' + \mu_{tr} \quad (7)$$

where μ_{tr} and σ_{tr} are the mean and standard deviation of the training set.

3.3. Primary Visual Feature Guidance

The LDM uses the decoded \hat{z}'' and \hat{c}'' as key materials to generate images that exhibit semantic similarities to the ground truth. However, the fidelity of these reconstructions to details is limited. NeuralDiffuser proposes a primary visual feature guidance \hat{g}'' to solve the challenge.

Universal Guided Reconstruction: Score-based diffusion model derived in Song et al. (2021) defines a stochastic differential equation of the reverse diffusion process:

$$dz = [f(z, t) - g^2(t)s(z_t)]dt + g(t)d\bar{w} \quad (8)$$

where $s(z_t) = \nabla_{z_t} \log p(z_t)$ is the score function providing the generative tendency. Considering a conditional probability $p(z_t|y)$, the score function $s(z_t, y)$ can be derived by Bayes' rule as:

$$\begin{aligned} s(z_t, y) &= \nabla_{z_t} \log p(z_t|y) \\ &= \nabla_{z_t} \log p(z_t) + \nabla_{z_t} \log p(y|z_t) \end{aligned} \quad (9)$$

where $\nabla_{z_t} \log p(y|z_t)$ defines a classifier guidance (Dhariwal & Nichol, 2021). We generalize the classifier $\log p(y|z_t)$ to a universal guidance function:

$$s(z_t, g) = \nabla_{z_t} \log p(z_t) - \nabla_{z_t} \mathcal{L}_g(z_t, g) \quad (10)$$

We expect pre-trained models to serve as guidance functions. However, general pre-trained models cannot input high-noise images that are guided outside the natural image distribution. In NeuralDiffuser, we estimate the clean image from the noisy image using Tweedie's method (Efron, 2011; Kim & Ye, 2021) and obtain the final image using a weight formula with Euler's formula approximation.

$$\hat{z}_0 := \mathbb{E}[z_0|z_t] = \frac{1}{\sqrt{\bar{\alpha}_t}}(z_t + (1 - \bar{\alpha}_t)s(z_t)) \quad (11)$$

$$\hat{z}_t = \sqrt{1 - \bar{\alpha}_t}\hat{z}_0 + (1 - \sqrt{1 - \bar{\alpha}_t})z_t \quad (12)$$

Algorithm 1 primary visual feature guidance algorithm

Input: $z_0 = \hat{z}'', \hat{c}'', \hat{g}'', \kappa, \eta$

Initialize: $z_T \leftarrow \sqrt{\bar{\alpha}_T}z_0 + \sqrt{1 - \bar{\alpha}_T}\epsilon$

for $t = T \rightarrow 1$ **do**

$$\hat{z}_0 = \frac{1}{\sqrt{\bar{\alpha}_t}}(z_t + (1 - \bar{\alpha}_t)\nabla_{z_t} \log p(z_t))$$

if $t < \eta T$ **then**

$$\hat{z}_t = \sqrt{1 - \bar{\alpha}_t}\hat{z}_0 + (1 - \sqrt{1 - \bar{\alpha}_t})z_t$$

$$\mathcal{L}_g(\hat{z}_t, \hat{g}'') = \kappa \cdot \|f_g^*(\mathcal{D}(\hat{z}_t)) - \hat{g}''\|_2^2$$

$$\hat{c} = \epsilon_\theta(z_t, \hat{c}'') + \sqrt{1 - \bar{\alpha}_t}\nabla_{z_t} \mathcal{L}_g(\hat{z}_t, \hat{g}'')$$

$$z_{t-1} = \sqrt{\bar{\alpha}_{t-1}}\left(\frac{z_t - \sqrt{1 - \bar{\alpha}_t}\hat{c}}{\sqrt{\bar{\alpha}_t}}\right) + \sqrt{1 - \bar{\alpha}_{t-1}}\hat{c}$$

else

$$z_{t-1} = \sqrt{\bar{\alpha}_{t-1}}\hat{z}_0 + \sqrt{1 - \bar{\alpha}_{t-1}}\epsilon_\theta(z_t, \hat{c}'')$$

end if

end for

Primary Visual Feature Decoding: There are numerous guidances, such as skeleton, object detection, semantic segmentation, etc, has been developed in the field of Computer Vision(CV). However, decoding the above guidance from fMRI poses challenges, including poor accuracy and complex decoders. In our work, we gain insights from voxel-wise predictions obtained by comparing multiple layers of the CLIP visual encoder with the cerebral cortex(including early visual cortex)(Wang et al., 2023). Therefore, NeuralDiffuser uses the embeddings of multiple layers (layer-2,4,6,8,10,12) in CLIP visual encoder as guided features:

$$g_i^n = CLIP_{image}(y_i, L^n), \quad n = 2, 4, 6, 8, 10, 12 \quad (13)$$

where L^n is the n -th layer of CLIP visual encoder.

To decode \hat{g}'' from fMRI, the f_g adopts a similar architecture as f_c because of the similar sizes of $g^n \in \mathbb{R}^{50 \times 768}$ and $c \in \mathbb{R}^{77 \times 768}$.

Primary Visual Feature-Guided Reconstruction: To reconstruct visual images with guidance, we use stable-diffusion-v1-4 with \hat{z}'' as the initial latent, \hat{c}'' as the semantic condition and guided by \hat{g}'' .

We aims to reconstruct the visual stimuli rather than generating different images, which is extremely deviates from the original intention of guided diffusion in CV. For this, we propose a novel guidance strategy. Firstly, we introduce a large guidance scale, $\kappa = 500k$ in NeuralDiffuser, as a strong constraint to ensure consistent results (see Figure 6):

$$\mathcal{L}_g(z_t, g) = \kappa \cdot \|f_g^*(\mathcal{D}(\hat{z}_t)) - \hat{g}''\|_2^2 \quad (14)$$

where \mathcal{D} is the VQ-VAE's decoder.

However, due to \hat{g}'' being decoded from fMRI instead of explicitly defined visual semantics, the manifold of gradients becomes discontinuous and is adversely affected by large guidance scales. In practice, we observed that reconstructed images exhibit artifacts and blur (see $\eta = 1.0$ in Figure 7).



Figure 4. Comparison for NeuralDiffuser with the state-of-the-art methods

Our solution based on the observation that primary visual feature guidance focuses on the early steps of the reverse diffusion process. We introduce a hyperparameter η to control the guidance rate of full steps. NeuralDiffuser adopts a small $\eta = 0.2$ since the primary features are corrected within few steps as shown in Fig 2. The total algorithm is described in Algorithm 1.

4. Experiments

4.1. Experimental Setup

Dataset: We evaluate NeuralDiffuser on the Natural Scenes Dataset (NSD) (Allen et al., 2022) where 73,000 images were viewed by 8 subjects. Each subject was assigned 10,000 images, including 9,000 unique images and 1,000 shared images. We trained subject-dependent decoders for 4 subjects (subj01, subj02, subj05, subj07). 24,980 trials were taken from 9,000 unique images as the training set (24,980 training samples) and the remaining 2,770 trials were averaged over 3 replicates as the test set (982 test samples). See Appendix A.3 for more details.

Metrics: Following previous research (Scotti et al., 2023; Xia et al., 2023), we use 8 metrics for quantitative comparison. More details in Appendix A.4. In addition, we use Inception Score (IS) (Salimans et al., 2016) and Fréchet Inception Distance (FID) (Seitzer, 2020) to evaluate the generated image quality.

Implementation: Our training and inference are deployed on an NVIDIA GeForce RTX 3090 GPU. We use stable-diffusion-v1-4 and DDIMSampler to generate images with 50 steps. We set the guidance hyperparameters $\kappa = 500k$ and $\eta = 0.2$ unless otherwise specified. See Appendix A.2 for more details.

4.2. fMRI Embeddings Decoding

Decoding fMRI embeddings \hat{z} , \hat{c} , and \hat{g} is a crucial step in fMRI reconstruction. The decoding accuracy is evaluated as the Pearson correlation between fMRI embeddings

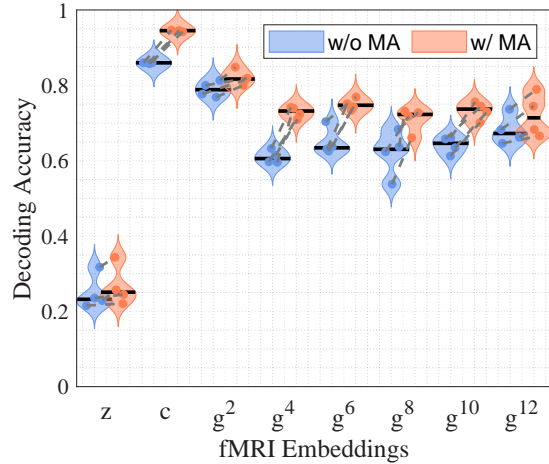


Figure 5. Decoding accuracy of fMRI embeddings. MA denotes momentum alignment.

and the ground truth. As depicted in Figure 5, NeuralDiffuser achieves remarkable decoding accuracy in semantic conditions \hat{c} and guidance \hat{g} , except for the initial latent \hat{z} .

Note that the poor decoding performance of \hat{z} is not unique to NeuralDiffuser, but rather a common problem encountered in previous studies, which often results in blurry initial reconstructions. We attribute the poor performance of \hat{z} not only to the complexity of decoding the early visual cortex, but also to the discretization of the VQ-VAE’s latent space. NeuralDiffuser takes another way by using the primary visual feature guidance to provide the detail cues, which compensate for the poor decoding performance of the initial latent \hat{z} by incorporating a well-decoded guidance \hat{g} .

4.3. Reconstruction

Comparison with State-of-the-Art: NeuralDiffuser is compared to 7 state-of-the-art methods. For each test image, we repeatedly generated five images and averaged them to obtain quantitative results. We finally report average results across 4 subjects. The qualitative evaluation, as presented in Figure 4, indicates that NeuralDiffuser is significantly superior to others, particularly for low-level details such as

Table 1. Reconstruction results of NeuralDiffuser (Top) and ablation study (Bottom)

Method	Low-Level				High-Level			
	SSIM \uparrow	Pixcorr \uparrow	AlexNet(2) \uparrow	AlexNet(5) \uparrow	CLIP \uparrow	Inception \uparrow	EffNet \downarrow	SwAV \downarrow
Mind-Reader (2022)	–	–	–	–	–	78.2%	–	–
Takagi <i>et al.</i> (2023)	–	–	83.0%	83.0%	77.0%	76.0%	–	–
MindDiffuser (2023)	.354	.278	–	–	76.5%	–	–	–
Brain-Diffuser (2023)	.356	.254	94.2%	96.2%	91.5%	87.2%	.775	.423
MindEye (2023)	.323	.309	94.7%	97.8%	94.1%	93.8%	.645	.367
DREAM (2023)	.338	.288	93.9%	96.7%	94.1%	93.7%	.645	.418
MindEye+BOI (2023)	.329	.259	93.9%	97.7%	93.9%	93.9%	.645	.367
NeuralDiffuser (Ours)	.328	.370	99.1%	99.5%	97.7%	98.0%	.626	.293
– guidance $\{\hat{z}'', \hat{c}''\}$.293	.287	89.0%	93.1%	96.8%	96.8%	.644	.309
– momentum alignment $\{\hat{z}, \hat{c}\}$.346	.244	85.6%	89.0%	93.7%	93.4%	.815	.451
groundtruth $\{z, c\}$.380	.681	100.0%	100.0%	99.7%	99.8%	.453	.191
+ guidance $\{z, c, g\}$.421	.771	100.0%	100.0%	99.9%	99.9%	.361	.158

structure, background, texture, color, etc. From the quantitative evaluation shown in Table 1 (top), we conclude that NeuralDiffuser outperforms the state-of-the-art at both the low and high level performance.

Low-level improvements are foreseeable as our proposed primary visual feature guidance provides detail cues and controls the reverse diffusion process. Surprisingly, the high level has also improved. It indicates that NeuralDiffuser has the ability to extract high-level semantic knowledge from low-level details, which reflects a bottom-up process. Thus, NeuralDiffuser is consistent with neuroscience theory. See Appendix B.2 for more results of 4 subjects, reseparately.

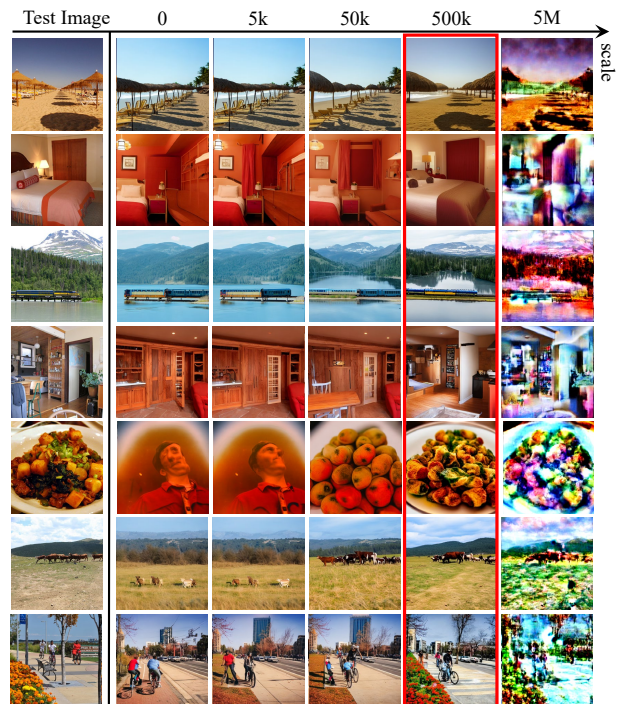
4.4. Ablation Study

Here, we present the ablation study on the momentum alignment and primary visual feature guidance. Furthermore, we also discuss the hyperparameters κ and strength η utilized in the guidance algorithm.

Effect of the Proposed:

Table 1 (bottom) demonstrates the results obtained by ablating the momentum alignment and primary visual feature guidance. Firstly, ablating the guidance leads to a deterioration in performance, both in terms of low and high levels. The decline in low-level metrics is mainly due to the lack of detail cues in reverse diffusion process that generate images conditional on semantic \hat{c}'' but do not depict detail. The decline in high-level metrics highlights the significance of bottom-up flow which is detail-driven visual cognition. An interesting observation is that the guidance even improves performance when used with ground truth embeddings, suggesting that our proposal works for the essential of LDM-based methods. Hence, it can serve as a general solution for any existing LDM-based reconstruction approach. Reconstructed images with and without guidance are present in Section 4.5 and Appendix B.1.

In addition, the ablation study on momentum alignment


 Figure 6. Different guidance scale κ ($\eta = 0.2$)

demonstrates that it effectively narrow the distribution distance between the training and test domain, resulting in a significant improvement in reconstruction performance.

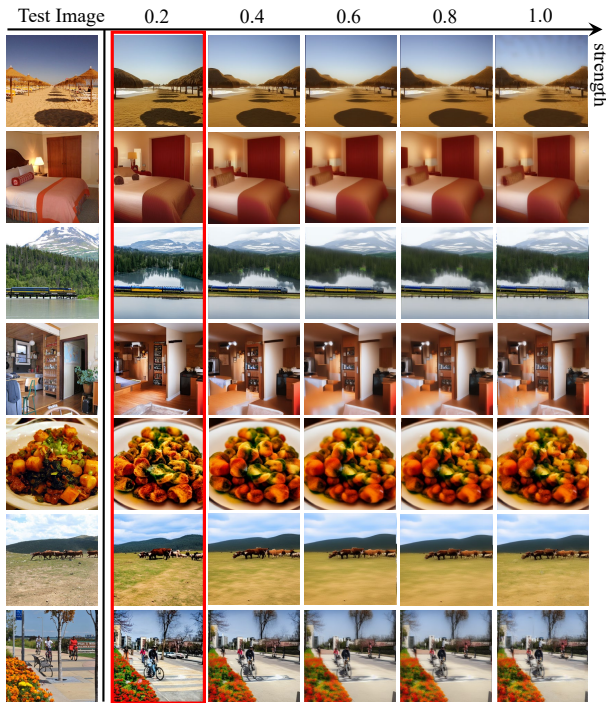
Adjustment of Guidance Scale κ & Strength η : Our proposed guidance sets two hyperparameters κ and η to adjust the scale and strength respectively, which mainly trade-off consistency and quality. Here, we evaluate the results of different κ and η .

First, we evaluate the performance of the different guidance scale κ qualitatively (Figure 6) and quantitatively (Table 2). We observed that a larger κ highlights the role of primary visual feature guidance, whereas an excessively large $\kappa = 5M$ leads to distortions because the fMRI embedding \hat{g}'' , is

Table 2. Results of different hyperparameters. guidance scale(Top) & strength(Bottom)

κ	η	Pixel			Low-Level		High-Level				Quality	
		SSIM \uparrow	Pixcorr \uparrow	RMSE \downarrow	Alex(2) \uparrow	Alex(5) \uparrow	CLIP \uparrow	IncepV3 \uparrow	EffNet \downarrow	SwAV \downarrow	IS \uparrow	FID \downarrow
5k	0.2	.295	.290	.320	89.9%	93.7%	96.8%	96.7%	.640	.306	31.3 \pm 1.23	64.5
50k	0.2	.305	.308	.314	94.1%	96.7%	97.1%	97.0%	.625	.292	31.0 \pm 1.12	63.9
500k	0.2	.328	.370	.303	99.1%	99.5%	97.7%	98.0%	.626	.293	27.8 \pm 0.99	69.9
1M	0.2	.322	.383	.308	99.5%	99.7%	97.2%	98.0%	.675	.337	22.6 \pm 0.73	83.4
5M	0.2	.247	–	.378	98.9%	99.5%	88.3%	91.0%	.896	.499	7.2 \pm 0.2	183.2

500k	0.2	.328	.370	.303	99.1%	99.5%	97.7%	98.0%	.626	.293	27.8 \pm 0.99	69.9
500k	0.4	.368	.410	.286	99.3%	99.6%	97.9%	98.0%	.654	.347	23.3 \pm 0.96	83.4
500k	0.6	.383	.429	.278	99.4%	99.6%	97.9%	97.7%	.693	.396	20.0 \pm 1.02	97.2
500k	0.8	.386	.437	.275	99.5%	99.6%	98.0%	97.8%	.694	.399	19.6 \pm 1.01	99.2
500k	1.0	.392	.442	.274	99.6%	99.8%	98.4%	98.4%	.662	.368	21.3 \pm 1.00	94.7


 Figure 7. Different guidance strength η ($\kappa = 500k$)

inaccurate and noisy. We use two metrics, Inception Score (IS) and Fréchet Inception Distance (FID), to measure image quality. We found that an excessively large $\kappa = 5M$ causes a notable decline in quality. As a compromise, we set the value of κ to $500k$ in this paper.

Furthermore, we observed that full-step guidance leads to blurry images as shown in Figure 7 ($\eta = 1.0$). We intuitively argue that it is caused by discontinuous guided gradients in the reverse diffusion process. Our solution is inspired by the insight that primary visual feature guidance focuses mainly on the beginning steps of the reverse diffusion process (see Figure 2). Therefore, we suggest that guidance be applied $\eta = 0.2 \times$ of the full step, while remaining $1 - \eta \times$ standard diffusion steps without guidance to ensure a clear output. As quantitative evaluation is presented in Table 2, a larger η improves the metrics but reduces image quality. Note that it



Figure 8. Five repeated reconstructed images (reconstructed by GT: groundtruth embeddings, fMRI: fMRI embeddings)

provides a personalized option, enabling the use of a small η for high-quality and a large η for high fidelity. This paper suggests $\eta = 0.2$, as it is sufficient to correct blurry initial latents, despite a larger η leads to better metrics.

4.5. Reconstruction Consistency

Figure 8 showcases five repeated results. Without guidance, the LDM generates different results because of diversity, that is, the same condition can generate different images. In contrast, when employing guidance in the LDM, there is a notable improvement in consistency across the repeated results. For more reconstructed examples, see Appendix B.1.

5. Conclusion

For the challenges of detail fidelity and consistency of repeated results in fMRI reconstruction, this paper presents a neuroscientific perspective on LDM-based methods. We attribute unfaithful details in LDM-based methods to the lack of detail-driven bottom-up process. Considering these, we propose NeuralDiffuser, a primary visual feature-guided LDM-based fMRI reconstruction method that incorporates detail cues for achieving faithful semantics and details. Furthermore, we introduce a novel guidance strategy that utilizes hyperparameters κ and η to enhance the consistency of repeated results.

Acknowledgments

This work was supported by the National Natural Science Foundation of China Grant No.62311540022, No.U21A20485, and No.62088102.

References

- Allen, E. J., St-Yves, G., Wu, Y., Breedlove, J. L., Prince, J. S., Dowdle, L. T., Nau, M., Caron, B., Pestilli, F., Charest, I., et al. A massive 7t fmri dataset to bridge cognitive neuroscience and artificial intelligence. *Nature neuroscience*, 25(1):116–126, 2022.
- Bansal, A., Chu, H.-M., Schwarzschild, A., Sengupta, S., Goldblum, M., Geiping, J., and Goldstein, T. Universal guidance for diffusion models. In *Proceedings of the IEEE/CVF Conference on Computer Vision and Pattern Recognition*, pp. 843–852, 2023.
- Beliy, R., Gaziv, G., Hoogi, A., Strappini, F., Golan, T., and Irani, M. From voxels to pixels and back: Self-supervision in natural-image reconstruction from fmri. *Advances in Neural Information Processing Systems*, 32, 2019.
- Caron, M., Misra, I., Mairal, J., Goyal, P., Bojanowski, P., and Joulin, A. Unsupervised learning of visual features by contrasting cluster assignments. *Advances in neural information processing systems*, 33:9912–9924, 2020.
- Chen, Z., Qing, J., Xiang, T., Yue, W. L., and Zhou, J. H. Seeing beyond the brain: Conditional diffusion model with sparse masked modeling for vision decoding. In *Proceedings of the IEEE/CVF Conference on Computer Vision and Pattern Recognition*, pp. 22710–22720, 2023.
- Dhariwal, P. and Nichol, A. Diffusion models beat gans on image synthesis. *Advances in neural information processing systems*, 34:8780–8794, 2021.
- Efron, B. Tweedie’s formula and selection bias. *Journal of the American Statistical Association*, 106(496):1602, 2011.
- Felleman, D. J. and Van Essen, D. C. Distributed hierarchical processing in the primate cerebral cortex. *Cerebral cortex (New York, NY: 1991)*, 1(1):1–47, 1991.
- Friston, K. A theory of cortical responses. *Philosophical transactions of the Royal Society B: Biological sciences*, 360(1456):815–836, 2005.
- Gilbert, C. D. and Sigman, M. Brain states: top-down influences in sensory processing. *Neuron*, 54(5):677–696, 2007.
- Goodfellow, I., Pouget-Abadie, J., Mirza, M., Xu, B., Warde-Farley, D., Ozair, S., Courville, A., and Bengio, Y. Generative adversarial nets. *Advances in neural information processing systems*, 27, 2014.
- Güçlü, U. and van Gerven, M. A. Deep neural networks reveal a gradient in the complexity of neural representations across the ventral stream. *Journal of Neuroscience*, 35(27):10005–10014, 2015.
- Henderson, M. M., Tarr, M. J., and Wehbe, L. Low-level tuning biases in higher visual cortex reflect the semantic informativeness of visual features. *Journal of Vision*, 23(4):8–8, 2023.
- Ho, J. and Salimans, T. Classifier-free diffusion guidance. *arXiv preprint arXiv:2207.12598*, 2022.
- Horikawa, T. and Kamitani, Y. Generic decoding of seen and imagined objects using hierarchical visual features. *Nature communications*, 8(1):15037, 2017.
- Ju, X., Zeng, A., Zhao, C., Wang, J., Zhang, L., and Xu, Q. Humansd: A native skeleton-guided diffusion model for human image generation. *arXiv preprint arXiv:2304.04269*, 2023.
- Karras, T., Aittala, M., Hellsten, J., Laine, S., Lehtinen, J., and Aila, T. Training generative adversarial networks with limited data. *Advances in neural information processing systems*, 33:12104–12114, 2020a.
- Karras, T., Laine, S., Aittala, M., Hellsten, J., Lehtinen, J., and Aila, T. Analyzing and improving the image quality of stylegan. In *Proceedings of the IEEE/CVF conference on computer vision and pattern recognition*, pp. 8110–8119, 2020b.
- Kietzmann, T. C., Spoerer, C. J., Sörensen, L. K., Cichy, R. M., Hauk, O., and Kriegeskorte, N. Recurrence is required to capture the representational dynamics of the human visual system. *Proceedings of the National Academy of Sciences*, 116(43):21854–21863, 2019.
- Kim, K. and Ye, J. C. Noise2score: tweedie’s approach to self-supervised image denoising without clean images. *Advances in Neural Information Processing Systems*, 34: 864–874, 2021.
- Kim, S., Lee, G., Bae, S., and Yun, S.-Y. Mixco: Mix-up contrastive learning for visual representation. *arXiv preprint arXiv:2010.06300*, 2020.
- Kingma, D. P. and Welling, M. Auto-encoding variational bayes. *arXiv preprint arXiv:1312.6114*, 2013.
- Kneeland, R., Ojeda, J., St-Yves, G., and Naselaris, T. Brain-optimized inference improves reconstructions of fmri brain activity. *arXiv preprint arXiv:2312.07705*, 2023.

- Krizhevsky, A., Sutskever, I., and Hinton, G. E. Imagenet classification with deep convolutional neural networks. *Advances in neural information processing systems*, 25, 2012.
- Lin, S., Sprague, T., and Singh, A. K. Mind reader: Reconstructing complex images from brain activities. *Advances in Neural Information Processing Systems*, 35: 29624–29636, 2022.
- Lin, T.-Y., Maire, M., Belongie, S., Hays, J., Perona, P., Ramanan, D., Dollár, P., and Zitnick, C. L. Microsoft coco: Common objects in context. In *Computer Vision—ECCV 2014: 13th European Conference, Zurich, Switzerland, September 6–12, 2014, Proceedings, Part V 13*, pp. 740–755. Springer, 2014.
- Lin, Y., Li, J., and Wang, H. Dcnn-gan: Reconstructing realistic image from fmri. In *2019 16th International Conference on Machine Vision Applications (MVA)*, pp. 1–6. IEEE, 2019.
- Lu, Y., Du, C., Zhou, Q., Wang, D., and He, H. Mind-diffuser: Controlled image reconstruction from human brain activity with semantic and structural diffusion. In *Proceedings of the 31st ACM International Conference on Multimedia*, pp. 5899–5908, 2023.
- Mou, C., Wang, X., Xie, L., Zhang, J., Qi, Z., Shan, Y., and Qie, X. T2i-adapter: Learning adapters to dig out more controllable ability for text-to-image diffusion models. *arXiv preprint arXiv:2302.08453*, 2023.
- Ozcelik, F. and VanRullen, R. Brain-diffuser: Natural scene reconstruction from fmri signals using generative latent diffusion. *arXiv preprint arXiv:2303.05334*, 2023.
- Ozcelik, F., Choksi, B., Mozafari, M., Reddy, L., and VanRullen, R. Reconstruction of perceived images from fmri patterns and semantic brain exploration using instance-conditioned gans. In *2022 International Joint Conference on Neural Networks (IJCNN)*, pp. 1–8. IEEE, 2022.
- Perarnau, G., Van De Weijer, J., Raducanu, B., and Álvarez, J. M. Invertible conditional gans for image editing. *arXiv preprint arXiv:1611.06355*, 2016.
- Pollen, D. A. On the neural correlates of visual perception. *Cerebral cortex*, 9(1):4–19, 1999.
- Qian, C., Sun, X., Wang, Y., Zheng, X., Wang, Y., and Pan, G. Binless kernel machine: Modeling spike train transformation for cognitive neural prostheses. *Neural Computation*, 32(10):1863–1900, 2020.
- Radford, A., Kim, J. W., Hallacy, C., Ramesh, A., Goh, G., Agarwal, S., Sastry, G., Askell, A., Mishkin, P., Clark, J., et al. Learning transferable visual models from natural language supervision. In *International conference on machine learning*, pp. 8748–8763. PMLR, 2021.
- Ramesh, A., Dhariwal, P., Nichol, A., Chu, C., and Chen, M. Hierarchical text-conditional image generation with clip latents. *arXiv preprint arXiv:2204.06125*, 1(2):3, 2022.
- Ren, Z., Li, J., Xue, X., Li, X., Yang, F., Jiao, Z., and Gao, X. Reconstructing seen image from brain activity by visually-guided cognitive representation and adversarial learning. *NeuroImage*, 228:117602, 2021.
- Rombach, R., Blattmann, A., Lorenz, D., Esser, P., and Ommer, B. High-resolution image synthesis with latent diffusion models. In *Proceedings of the IEEE/CVF conference on computer vision and pattern recognition*, pp. 10684–10695, 2022.
- Rossion, B., Bodart, J.-M., Pourtois, G., Thioux, M., Bol, A., Cosnard, G., Georges, B., Michel, C., and De Volder, A. Functional imaging of visual semantic processing in the human brain. *Cortex*, 36(4):579–591, 2000.
- Salimans, T., Goodfellow, I., Zaremba, W., Cheung, V., Radford, A., and Chen, X. Improved techniques for training gans. *Advances in neural information processing systems*, 29, 2016.
- Scotti, P. S., Banerjee, A., Goode, J., Shabalin, S., Nguyen, A., Cohen, E., Dempster, A. J., Verlinde, N., Yundler, E., Weisberg, D., et al. Reconstructing the mind’s eye: fmri-to-image with contrastive learning and diffusion priors. *arXiv preprint arXiv:2305.18274*, 2023.
- Seeliger, K., Güçlü, U., Ambrogioni, L., Güçlütürk, Y., and van Gerven, M. A. Generative adversarial networks for reconstructing natural images from brain activity. *NeuroImage*, 181:775–785, 2018.
- Seitzer, M. pytorch-fid: FID Score for PyTorch. <https://github.com/mseitzer/pytorch-fid>, August 2020. Version 0.3.0.
- Shen, G., Dwivedi, K., Majima, K., Horikawa, T., and Kamitani, Y. End-to-end deep image reconstruction from human brain activity. *Frontiers in computational neuroscience*, 13:21, 2019.
- Song, Y., Sohl-Dickstein, J., Kingma, D. P., Kumar, A., Ermon, S., and Poole, B. Score-based generative modeling through stochastic differential equations. In *International Conference on Learning Representations*, 2021. URL <https://openreview.net/forum?id=PxtTIG12RRHS>.

- St-Yves, G. and Naselaris, T. Generative adversarial networks conditioned on brain activity reconstruct seen images. In *2018 IEEE international conference on systems, man, and cybernetics (SMC)*, pp. 1054–1061. IEEE, 2018.
- Szegedy, C., Vanhoucke, V., Ioffe, S., Shlens, J., and Wojna, Z. Rethinking the inception architecture for computer vision. In *Proceedings of the IEEE conference on computer vision and pattern recognition*, pp. 2818–2826, 2016.
- Takagi, Y. and Nishimoto, S. High-resolution image reconstruction with latent diffusion models from human brain activity. In *Proceedings of the IEEE/CVF Conference on Computer Vision and Pattern Recognition*, pp. 14453–14463, 2023a.
- Takagi, Y. and Nishimoto, S. Improving visual image reconstruction from human brain activity using latent diffusion models via multiple decoded inputs. *arXiv preprint arXiv:2306.11536*, 2023b.
- Tan, M. and Le, Q. Efficientnet: Rethinking model scaling for convolutional neural networks. In *International conference on machine learning*, pp. 6105–6114. PMLR, 2019.
- Voynov, A., Aberman, K., and Cohen-Or, D. Sketch-guided text-to-image diffusion models. In *ACM SIGGRAPH 2023 Conference Proceedings*, pp. 1–11, 2023.
- Wang, A. Y., Kay, K. N., Naselaris, T., Tarr, M. J., and Wehbe, L. Natural language supervision with a large and diverse dataset builds better models of human high-level visual cortex. *bioRxiv*, 2023. URL <https://api.semanticscholar.org/CorpusID:259858715>.
- Wang, Z., Bovik, A. C., Sheikh, H. R., and Simoncelli, E. P. Image quality assessment: from error visibility to structural similarity. *IEEE transactions on image processing*, 13(4):600–612, 2004.
- Wen, H., Shi, J., Zhang, Y., Lu, K.-H., Cao, J., and Liu, Z. Neural encoding and decoding with deep learning for dynamic natural vision. *Cerebral cortex*, 28(12):4136–4160, 2018.
- Xia, W., de Charette, R., Öztireli, C., and Xue, J.-H. Dream: Visual decoding from reversing human visual system. *arXiv preprint arXiv:2310.02265*, 2023.
- Zhang, L., Rao, A., and Agrawala, M. Adding conditional control to text-to-image diffusion models. In *Proceedings of the IEEE/CVF International Conference on Computer Vision*, pp. 3836–3847, 2023.
- Zhao, S., Chen, D., Chen, Y.-C., Bao, J., Hao, S., Yuan, L., and Wong, K.-Y. K. Uni-controlnet: All-in-one control to text-to-image diffusion models. *arXiv preprint arXiv:2305.16322*, 2023.
- Zheng, G., Zhou, X., Li, X., Qi, Z., Shan, Y., and Li, X. Layoutdiffusion: Controllable diffusion model for layout-to-image generation. In *Proceedings of the IEEE/CVF Conference on Computer Vision and Pattern Recognition*, pp. 22490–22499, 2023.

A. Additional Method Details

A.1. Human Visual Cognition

A comprehensive understanding of how the brain generates visual cognition requires elucidate the dynamic connections, both bottom-up and top-down, within and between the neural structures involved. At the core of the top-down process is the idea that our brains actively interpret and make sense of the incoming stimuli based on pre-existing knowledge. This knowledge-driven approach relies heavily on our prior knowledge, experience, and expectations (Gilbert & Sigman, 2007). The bottom-up process represents a well-known pathway, i.e., visual signals deriving from the retina travel through the lateral geniculate nucleus in the thalamus to the visual cortex, where they diverge into two streams and undergo hierarchical processing from lower to higher cortical areas.. It is data-driven and relies heavily on the details coming in through our senses. Although we do not know how much of visual perception is directly due to sensation and how much is due to experience and training, it is evident that both factors play a role in the process of visual cognition (Pollen, 1999).

The structure of the visual cortex can be conceptualized as a hierarchy of cortical layers with reciprocal cortico-cortical connections between the constituent cortical areas (Felleman & Van Essen, 1991). Low-level cortical areas excel at processing direct light sensing, whereas high-level cortical areas excel at comprehending image semantics (Pollen, 1999). Studies indicate that low-level feature selectivity plays a crucial role in computing high-level semantics, while the statistics of primary visual features are modulated by semantic content (Henderson et al., 2023). As a specific example, outdoor scene images often exhibit prominent horizontal orientations and high spatial frequencies. These observations indicate that the two aforementioned processes can synergistically contribute to a more comprehensive understanding of various visual stimuli. The top-down process entails starting with an abstract concept and progressively zooming in on details, while bottom-up processes initiate with specific details and iteratively validate the concept at each level, incorporating experienced materials (Friston, 2005).

A.2. Implementation Details

The hyperparameter α is set to 0.03 for training the f_c and f_g models. We adopt AdamW optimizer and a cycle lr_schedule with a maximum learning rate of $3e-4$. Training is conducted on a single NVIDIA GeForce RTX 3090 for 100 epochs, employing a batch size of 32. Regarding z , we replicated the results published by MindEye (Scotti et al., 2023) because all implementations are the same. We additionally implemented momentum alignment to align distributions between the training set and test set.

We utilize `stable-diffusion-v1-4` to generate images with a size of 512×512 . We use 50 steps `DDIMSampler` and reverse diffusion strength of 0.75 (37 steps). By default, we set the classifier-free scale to 7.5, guidance scale κ to 500,000 and guidance strength η to 0.2. Since guidance involves gradient propagation, we recommend a GPU VRAM of at least 24GB like the NVIDIA GeForce RTX 3090. We emphasize that guidance only exists in 20% ($\eta = 0.2$) of the reverse diffusion steps and therefore does not significantly increase the computational time cost.

A.3. NSD Dataset

The Natural Scenes Dataset (NSD) (Allen et al., 2022) includes a diverse collection of fMRI-image pairs from 8 subjects. The 73,000 images obtained from Common Objects in Context (COCO) dataset (Lin et al., 2014) were split into 8 sets for 8 subjects, and each set was assigned 10,000 images, including 9,000 unique images and 1,000 shared images. Each subject viewed 10,000 images repeated $3 \times$ in 30-40 sessions while implementing a 7T fMRI scan. We evaluated four subjects who completed all imaging sessions (subj01, subj02, subj05, and subj07). We scanned at 1pt8mm resolution and selected fMRI signals of voxels in the `nsdgeneral` ROI provided by the dataset. Due to data unavailability, each subject obtained a total of 27,750 trials out of 30,000 trials. Among them, 24,980 trials were taken from 9,000 unique images as the training set (24,980 training samples), while the remaining 2,770 trials were taken from 1,000 shared images and were averaged across three same-images as the test set (982 test samples).

A.4. Metrics

Following previous research (Scotti et al., 2023; Xia et al., 2023), we employ a set of 8 metrics for quantitative evaluation, including pixel-level correlation (PixCorr), Structural Similarity Index (SSIM) (Wang et al., 2004), AlexNet(2), AlexNet(5), CLIP, Inception, EffNet-B (Tan & Le, 2019), and SwAV (Caron et al., 2020). AlexNet(2) and AlexNet(5), as the low-level metrics, represent the two-way comparisons of the 2nd and 5th feature layers of AlexNet (Krizhevsky et al., 2012) respectively.

CLIP and Inception, as the high-level metrics, denote the two-way comparisons of the CLIP-Vision model(Radford et al., 2021) and the last pooling layer of InceptionV3(Szegedy et al., 2016), respectively. Furthermore, we employ Inception Score (IS)(Salimans et al., 2016) and Fréchet Inception distance (FID)(Seitzer, 2020) for evaluating the quality of the generated images.

A.5. fMRI Decoder Architecture

f_c : The semantic conditions c are extracted from CLIP text space, which has a size of $\mathbb{R}^{77 \times 768}$, where 77 represents the maximum token length and 768 denotes the feature dimension for each token. We propose mapping fMRI to CLIP text space because it focuses on explicit natural semantics while CLIP image space, with a size of $\mathbb{R}^{257 \times 768}$, also implies visual semantics(Rossion et al., 2000). On the other hand, decoders with low-dimensional embeddings tend to be smaller and perform better than high-dimensional embeddings. To map to the semantic conditions c , we adopt f_c which is followed from MindEye(Scotti et al., 2023). Specifically, it consists of an MLP backbone, a projector, and a diffusion prior. The MLP backbone, consisting of a linear layer followed by 4 residual blocks and a final linear layer, maps flattened voxels to a 77×768 dimensional vector. The backbone outputs are simultaneously fed to the projector and diffusion prior. The projector is a 3-layer MLP that produces elements for contrast loss. We execute a diffusion prior with 100 timesteps, and in this case, there are no learnable queries involved.

f_z : The initial latents z are extracted from VQ-VAE’s latent space with a size of $\mathbb{R}^{4 \times 64 \times 64}$ which denotes low-dimensional representations of images. To map to z , f_z uses an MLP backbone with 4 residual blocks that map fMRI to space with a size of $\mathbb{R}^{16 \times 16 \times 64}$. Subsequently, an upsampler, designed with a similar architecture to VQ-VAE decoder, is adopted to upsample backbone outputs to $\mathbb{R}^{64 \times 64 \times 4}$, which matches the dimensions of VQ-VAE’s latents.

f_g : The primary visual feature guidance g^n is extracted from the n -th layer of CLIP image encoder where $n = 2, 4, 6, 8, 10, 12$ with a size of $\mathbb{R}^{50 \times 768}$. For each g^n , f_g adopts the same architecture as f_c and the output size of MLP backbone is replaced by $\mathbb{R}^{50 \times 768}$ instead of $\mathbb{R}^{77 \times 768}$.

B. Additional Results

B.1. Repeat Multiple Generations

In our experimental setup, we repeatedly generate 5 reconstructed images for each test sample. Here, we present these 5 results of our experiments, showcasing the 5 reconstructed images both with and without the primary visual feature guidance.

$\{z, c, g\}$: First, we use groundtruth embeddings as the generative raw materials, which theoretically lead to an upper bound. The reconstructed images are present in Figure 9. The positions of elements in images without guidance exhibit variation even under the same semantic conditions. We attribute this phenomenon to the inherent diversity of the diffusion model. This paper proposes primary visual feature guidance to control the details including structure, background, texture, color, etc. The results obtained with guidance demonstrate a consistent pattern across the 5 repeated images. Results highlight the significant role played by primary visual feature guidance in the process of fMRI visual reconstruction.

$\{\hat{z}'', \hat{c}'', \hat{g}''\}$: we present more repeated reconstructed images in Figure 10. These results significantly demonstrate the efficacy of our proposal and showcase superior performance compared to other methods.

B.2. Results of 4 Subjects

We trained subject-dependent fMRI decoders on 4 subjects(S1, S2, S5, S7) reseparately. We report the results of NeuralDiffuser on 4 subjects in Table 3. For more reconstructed images, please refer to Figure 11 and Figure 12.

Table 3. Reconstruction results of NeuralDiffuser on multiple subjects

Method	Low-Level				High-Level			
	SSIM↑	Pixcorr↑	AlexNet(2)↑	AlexNet(5)↑	CLIP↑	Inception↑	EffNet↓	SwAV↓
subj01	.344	.456	99.9%	99.9%	98.2%	98.4%	.589	.266
subj02	.323	.361	99.2%	99.4%	97.2%	97.6%	.640	.304
subj05	.325	.335	98.8%	99.2%	97.6%	98.0%	.635	.297
subj07	.321	.326	98.4%	99.3%	97.8%	97.8%	.640	.303

NeuralDiffuser: Controllable fMRI Reconstruction with Primary Visual Feature Guided Diffusion

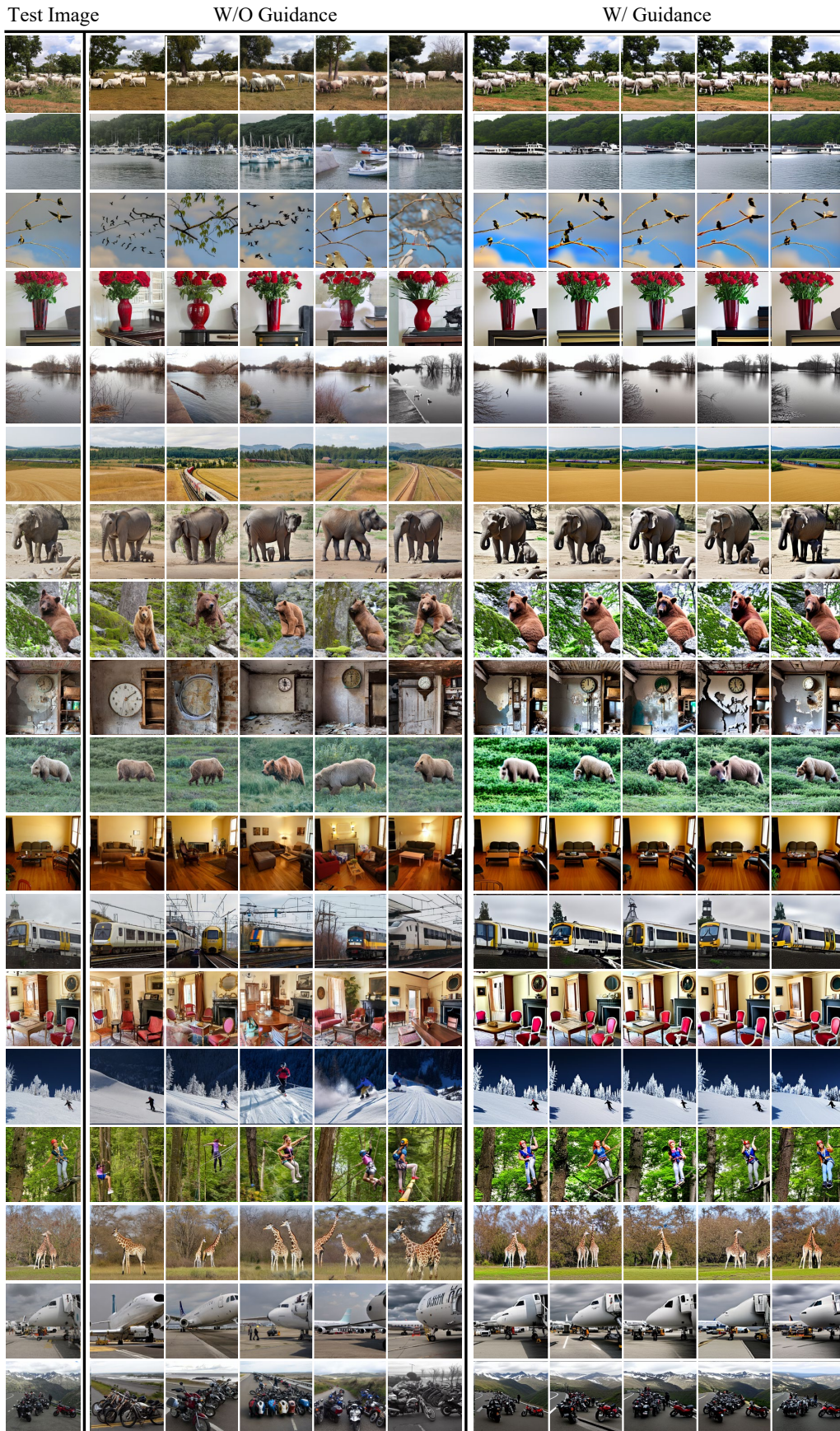


Figure 9. Five repeated reconstructed images of groundtruth embeddings

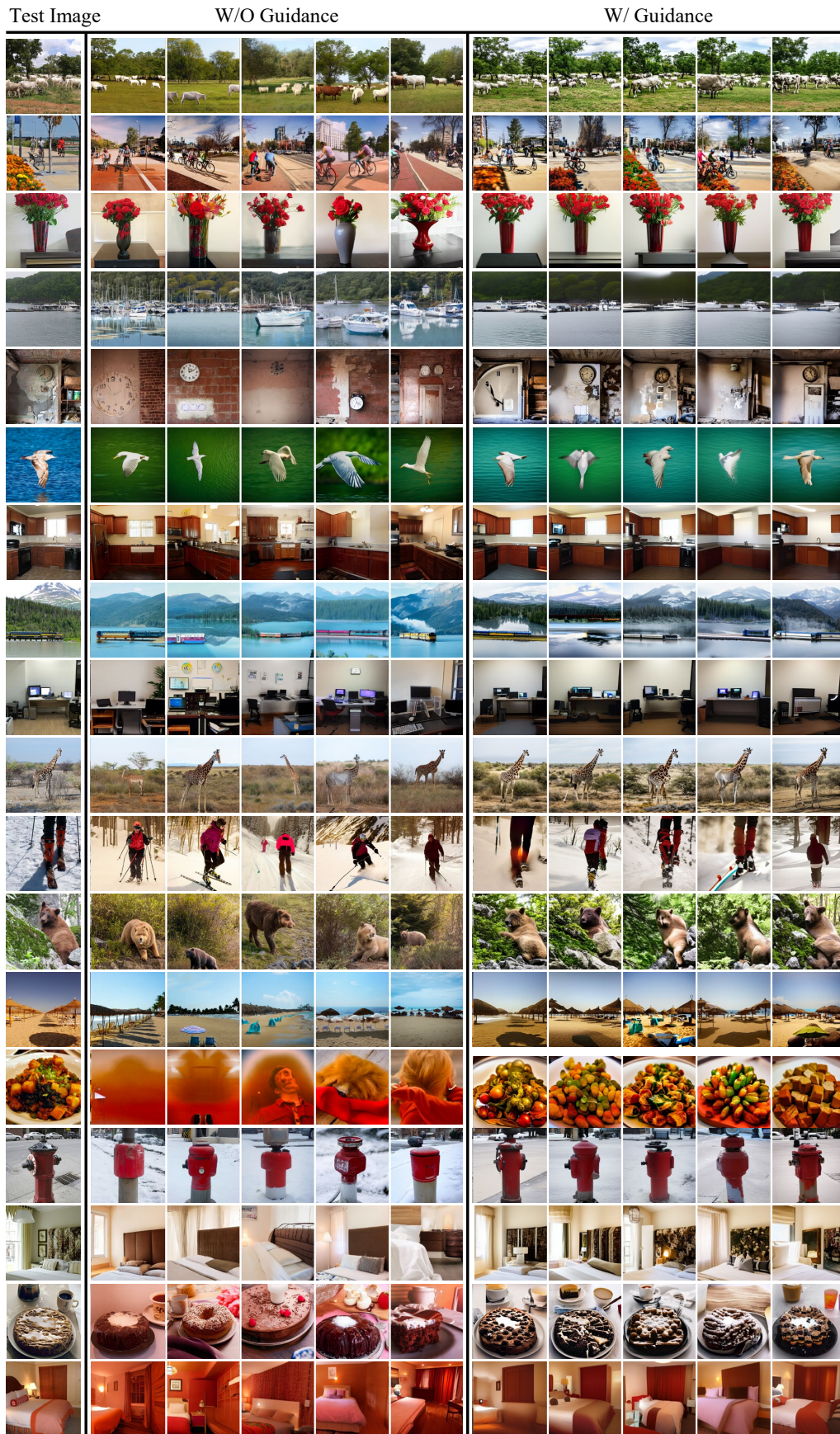


Figure 10. Five repeated reconstructed images of fMRI embeddings

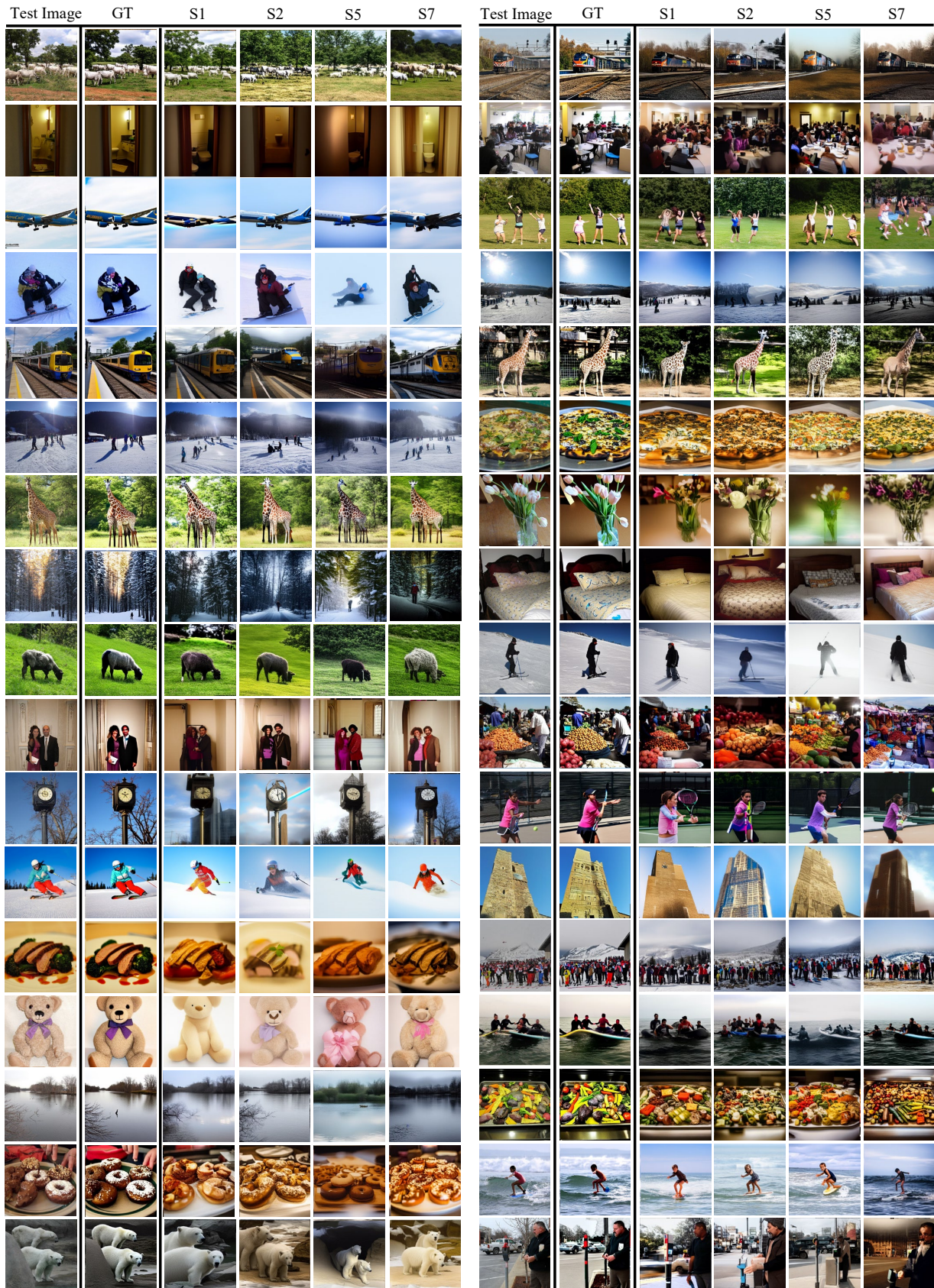


Figure 11. Reconstructed images of NeuralDiffuser on 4 subjects

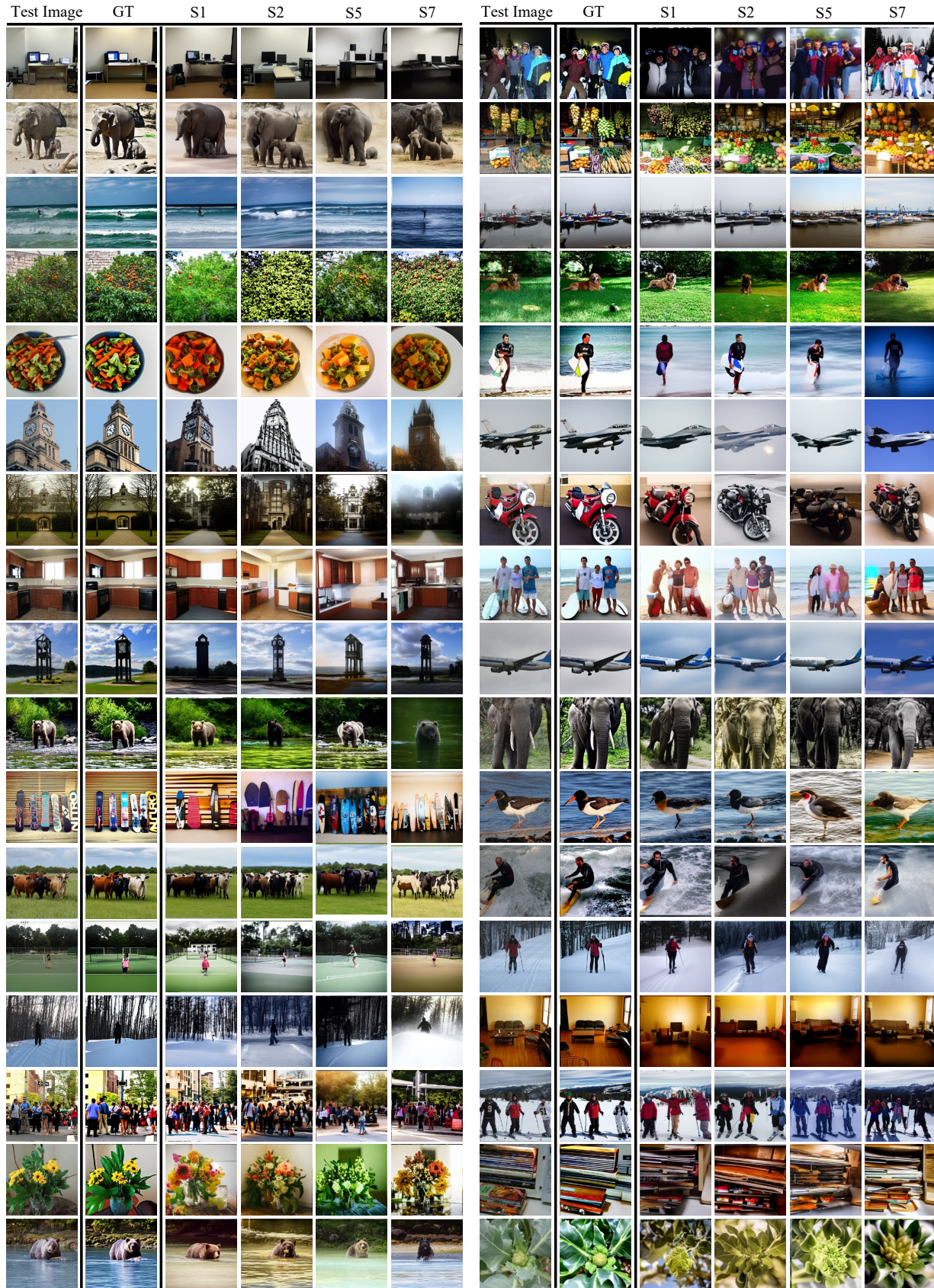


Figure 12. Reconstructed images of NeuralDiffuser on 4 subjects